NEW OBSERVATIONS OF HERBIG-HARO OBJECTS AND RELATED STARS[a)]

ROBERT W. GOODRICH
Lick Observatory, Board of Studies in Astronomy and Astrophysics, University of California, Santa Cruz, California 95064
Received 28 May 1986; revised 17 June 1986

ABSTRACT

Results of optical spectrophotometry are presented for several known and suspected Herbig-Haro (HH) objects and their parent stars. The optical spectrum of SSV 13, the parent star to the HH 7–11 chain, is presented for the first time. The object GGD 33a is shown to be reflecting light from the nearby T Tauri star V350 Cep, as well as producing some intrinsic emission. It is argued that Haro 6-10 is not an HH object in the normal sense of the term as a relatively isolated shock-excited nebulosity. Data on some other HH objects are also presented.

I. INTRODUCTION

The discovery and identification of Herbig-Haro objects is often constrained by the necessity of relying heavily on morphological criteria to make an initial cut. Subsequent to this definition of a morphological candidate list, spectra are obtained and the character of each target is determined. The original draft catalog of HH objects (Herbig 1974) contained objects both with and without spectra. Indeed, some of these objects are only now being studied spectroscopically. Two morphological lists obtained by studying the Palomar-National Geographic Sky Survey are the RNO (for "Red Nebulous Object"—Cohen 1980) and GGD (Gyul-'budagyan, Glushkov, and Denisyuk 1978, hereafter referred to as GGD78) catalogs. Subsequent spectroscopy of many of the objects from these latter two catalogs have shown a small fraction of objects which have the low-ionization forbidden-line spectrum characteristic of HH objects (see, for example, Cohen and Fuller 1985; Magakyan 1983). Other objects in these lists are reflection nebulae or stars embedded in nebulosity.

This contribution presents new spectrophotometry, spectropolarimetry, and imaging of several known and suspected HH objects and some of the stars believed to be associated with them.

II. OBSERVATIONS

The spectrophotometry was obtained with the transmission-optics Cassegrain spectrograph of the 3 m Shane reflector of Lick Observatory, using a virtual-phase Texas Instruments 800×800 pixel charge-coupled device (CCD) as the detector. A 420 line/mm grism gave a dispersion of 5.5 Å/pixel and a spectral resolution of 14 Å. A 2″-long slit was used, with each pixel perpendicular to the dispersion corresponding to 0″.73 on the sky. The spectra were reduced by standard methods using the image-processing program VISTA. Flux standards chosen from the lists of Stone (1974,1977) provided the absolute flux calibration.

The Cassegrain spectrograph was also used in its spectropolarimetry mode for some observations. Two generations of the spectropolarimeter were used. The first employed a piece of calcite to separate the two senses of polarization—the spectrograph was rotated to four different position angles to measure the Stokes parameters. The second generation utilized a Pockels cell in a manner very similar to that described by Miller, Robinson, and Schmidt (1980), except that the Pockels cell was used in an unmodulated mode. Both versions of the spectropolarimeter were double-beam instruments, a necessary feature for doing accurate spectropolarimetry. A 600 line/mm grism with a dispersion of 3.4 Å/pixel and a spectral resolution of 8 Å was used for the spectropolarimetry.

The Cassegrain spectrograph was also used in its imaging mode with the dispersing elements removed from the optical path. The direct CCD images were obtained through a broad-passband red filter described by Djorgovski (1985). Flat-field exposures produced by shining a tungsten light on the inside of the dome provide removal of the pixel-to-pixel sensitivity variations. The field of view of the system is approximately 2′ diameter, with each pixel having length 0″.73.

Table I presents the log of observations, listing the type of observation, the date, and the exposure time.

III. INDIVIDUAL OBJECTS

a) HH 7–11 and SSV 13

The well-studied string of HH objects HH 7–11 has been associated with the infrared source SSV 13 (Strom, Vrba, and Strom 1976). SSV 13 appears to be a highly reddened star, just visible on red CCD images of the region taken with the 1 m Anna Nickel telescope of Lick Observatory. The results of a single 1 hr, long-slit CCD spectrum of SSV 13, HH 8, HH 10, and HH 11 are presented in Fig. 1 and Tables

TABLE I. Log of observations.

Object	Observation type[a]	Date	Exposure time (m)
HH 7-11/SSV-13	S	21/22 Oct. 1984	60
GGD 33/V350 Cep	S	14/15 Jul. 1985	30
GGD 34,35	S	19/20 Aug. 1985	45
	I	19/20 Aug. 1985	3/5
Haro 6-10	SP	21/22 Jan. 1985	40
HH 40	SP	22/23 Jan. 1985	60
RNO 40	S	23/24 Jan. 1985	40

[a] S=spectrophotometry; SP=spectropolarimetry; I=image

[a)] Lick Observatory Bulletin No. 1048.

 0004-6256/86/040885-10$00.90

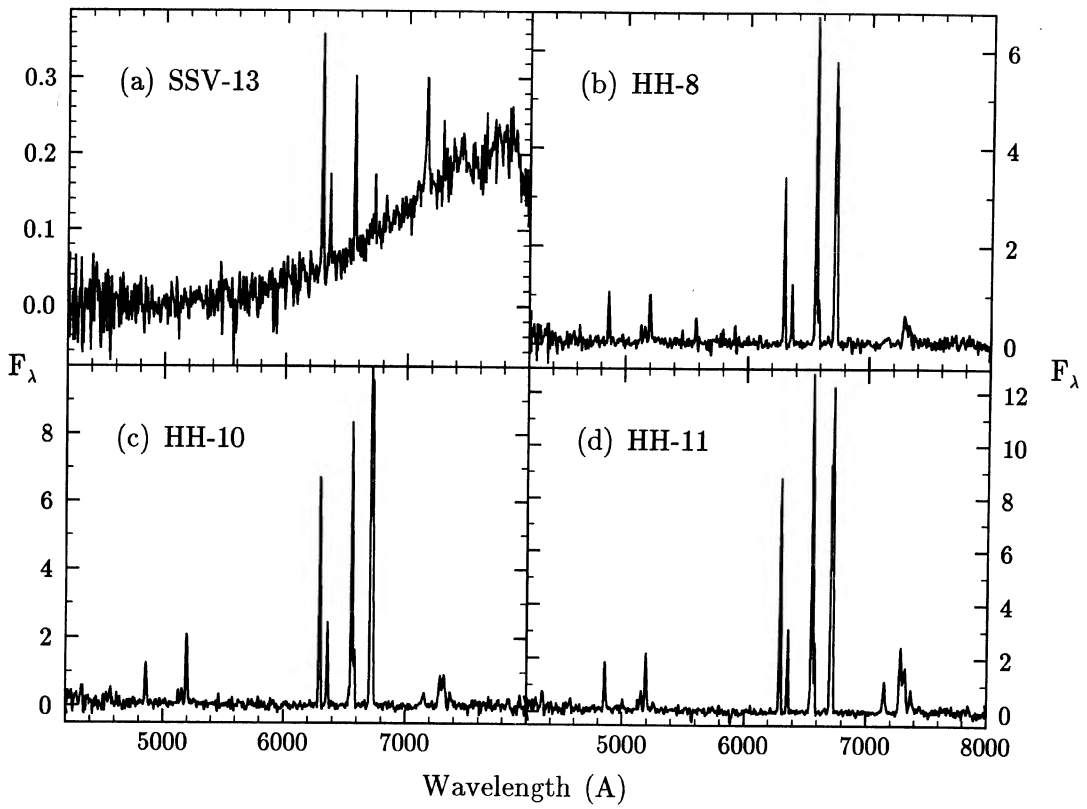

FIG. 1. Optical spectra of HH 8, HH 10, HH 11, and their parent star SSV 13. The units of F_λ are 10^{-16} erg cm^{-2} s^{-1} Å^{-1}.

II–IV. Figure 1(a) shows that the continuum of SSV 13 is very faint—$R \sim 20.3$ and $V \sim 23.8$ using monochromatic fluxes. The only features visible are the Hα λ 6563, [O I] $\lambda\lambda$ 6300, 6363, and [S II] $\lambda\lambda$ 6717, 6731 lines in emission. No absorption features attributable to TiO bands are seen, providing a weak constraint to the spectral type of the star—it must be spectral type K or earlier.

The emission spectrum of SSV 13 is similar to that of low-excitation HH objects in having strong [O I] lines with respect to Hα (see, however, the discussion in Sec. IV). This brings up the possibility that the image seen in the optical is not actually the star itself but simply a nebula shining partly by reflection (providing the red continuum) and partly by shock emission (providing the HH lines), analogous to the situation in parts of the HH 24 complex (Schmidt and Miller 1979). From a 60 min red image taken with a 386 × 576 pixel GEC CCD on the 1 m Nickel telescope, astrometry was performed to determine the position of the optical image. The restricted field of view contained only two stars, numbered 6 and 40 in Herbig and Jones (1983), but the star-like image of HH 11a was used to check the scale and relative rotation of the CCD image. The resulting position of the optical image near SSV 13 is $\alpha(1950) = 3^h25^m58^s.14$, $\delta(1950) = +31°05'45''.3$, with estimated uncertainties of 0".5 in each coordinate. This is consistent with the position of the infrared source as reported by, for example, Sandell and Olofsson (1981), and the position of the H_2O maser determined by Haschick *et al.* (1980). Regardless of the situation, the continuum represents a stellar component. The presence of HH emission in close proximity to SSV 13 could indicate that we are witnessing the birth of a new HH object in the HH 7–11 string. Long-term monitoring of the region, both by imaging and by spectroscopy, is clearly in order.

Figures 1(b)–1(d) present the spectra of HH 8, HH 10, and HH 11. The observed emission-line fluxes determined from these spectra are presented in Table II, while Table III lists the parameters of the shocks which are derived for the individual HH objects (using the models of Dopita 1977). The shock parameters were determined from the density-sensitive [S II] λ 6731/λ 6717 line ratio and the temperature-sensitive ratio of [O III] λ 5007/Hβ. Both of these line ratios are quite insensitive to reddening uncertainties. An intrinsic Hα/Hβ ratio was determined using the resulting values of N_e and T and was compared with the observed Hα/Hβ ratio to determine a reddening. The reddenings towards all three HH objects are consistent with a value of $E_{B-V} = 0.54$. The reddening towards the optical object at the position of SSV 13 may be estimated from its $V - R$ color of 3.5 mag. The intrinsic colors of the star are assumed to be those of a K star, with a luminosity class of either V or III. [The bolometric luminosity of 60 $L_\odot$ given by Cohen *et al.* (1984) is consistent with a K giant.] From Johnson (1967), the $V - R$ colors of stars within this range of parameters is 0.64 (for a K0 V) to 1.20 (for a K5 III), implying reddening values E_{B-V} of between 2.2 and 1.4. Hence, as noted by previous authors, the reddening towards the parent star is much higher than the reddening towards the HH objects.

Table IV presents measurements of the continuum fluxes in several wavelength regions for the HH objects. There is essentially no evidence for a reflected red continuum in any of these three HH objects, but there is a significant rise towards the blue, indicative of two-photon emission.

TABLE II. Emission of spectra.

Object	Flux (in units of 10^{-15} erg cm^{-2} s^{-1})													
	Hγ λ4340	Hβ λ4861	[O III] λ4959, 5007	[Fe II] λ5159	[N I] λ5199	[Fe II] λ5262	[O I] λ5577	[O I] λ6300, 6363	Hα λ6563	[N II] λ6584	[S II] λ6717	[S II] λ6731	[Fe II] λ7155	[Ca II] λ7300
HH-8	...	1.37	...	0.41	1.56	...	0.54	6.9	9.5	1.12	7.9	6.1	0.73	2.71
HH-10	...	1.80	...	0.58	3.6	...	...	13.4	11.9	2.06	14.0	13.9	1.05	4.0
HH-11	1.05	2.80	0.63	1.14	3.7	0.55	...	17.7	17.7	3.1	11.3	16.4	2.77	9.9
GGD 33a	...	0.13	...	0.16	...	0.12	...	2.46	2.97	...	0.22	0.42	0.52	...
GGD 33b	...	...	...	...	...	...	...	...	0.63	...	...	...	...	...
GGD 34	1.02	1.48	0.62	...	0.56	...	...	2.80	8.5	2.17	4.2	3.4	0.96	2.45
GGD 35	1.29	3.3	...	0.60	1.26	0.41	...	8.5	19.2	6.5	11.0	8.4	1.21	5.4
HH-40	...	15.9	14.5	2.63	4.8	1.64	1.46	17.6	92.	42.	44.	62.	...	...
RNO 40	8.1	21.1	6.9	7.2	8.2	4.8	1.13	79.	122.	45.	58.	71.	18.8	66.
SSV-13	...	...	...	...	...	...	...	0.56	0.30	...	0.06		0.35	...
V350 Cep	...	5.3	...	...	3.6	...	...	2.28	58.	...	...	...	...	...
Haro 6-10	...	5.4	0.93	...	...	...	...	19.9	112.	14.0	6.2	11.6	...	...

TABLE III. Shock parameters.

Object	Observed $\frac{\lambda 6731}{\lambda 6717}$	Observed $\frac{H\alpha}{H\beta}$	Observed $\frac{\lambda 5007}{H\beta}$	log N	log T	$\left(\frac{H\alpha}{H\beta}\right)_{int}$	E_{B-V}
HH-8	0.77	6.9	< 0.10	> 1.5	< 4.3	> 3.6	< 0.60
HH-10	0.99	6.6	< 0.11	> 2.1	< 4.4	> 3.6	< 0.56
HH-11	1.45	6.3	0.22	2.6	5.2	3.5	0.54
GGD 33a	1.91	22.8[a]	< 0.28	> 3.2	< 5.6	> 3.5	< 1.74
GGD 34	0.80	5.7	0.31	1.4	5.7	3.5	0.46
GGD 35	0.76	5.8	< 0.05	> 1.5	< 3.3	> 3.9	< 0.38
HH-40	1.38	5.8	0.24	2.3	5.3	3.4	0.49
RNO 40	1.22	5.8	0.24	2.3	5.3	3.5	0.46
Haro 6-10	1.86	20.8	0.13	3.2	4.6	3.6	1.63

[a] assuming that there is no [N II] in the Hα line.

TABLE IV. Continuum fluxes.

Object	F_λ in units of 10^{-17} erg cm^{-2} s^{-1} Å^{-1}									
	λλ4355–4845		λλ5300–5880		λλ5910–5985		λλ6380–6530		λλ6745–7100	
HH-8	0.61 ± 0.13		0.59 ± 0.10		0.47 ± 0.16		0.32 ± 0.07		0.23 ± 0.08	
HH-10	1.01	0.15	0.35	0.09	−0.05	0.26	0.20	0.12	0.03	0.08
HH-11	1.27	0.13	0.46	0.09	0.05	0.20	0.36	0.10	0.14	0.07
GGD 33a	0.27	0.03	0.65	0.03	0.78	0.05	1.12	0.04	1.20	0.03
GGD 33b	0.26	0.03	0.44	0.02	0.43	0.08	0.60	0.03	0.54	0.02
GGD 34	0.40	0.09	0.62	0.07	0.82	0.13	0.99	0.10	1.24	0.07
GGD 35	1.83	0.14	1.07	0.11	0.63	0.21	1.09	0.13	0.88	0.10
HH-40	3.98	0.74	3.23	0.21	3.73	0.35	2.11	0.45	...	
RNO 40	7.75	0.50	4.91	0.22	3.22	0.10	3.57	0.20	3.35	0.11
SSV-13	0.03	0.03	0.11	0.02	0.26	0.06	0.61	0.02	1.21	0.03
V350 Cep	34.3	0.4	54.7	0.3	55.5	0.4	75.8	0.8	85.7	1.1
Haro 6-10	14.1	0.5	56.1	1.0	83.8	0.5	131.7	1.4	...	

b) GGD 33a, 33b, and V350 Cep

The region around GGD 33 has been studied in the infrared by Cohen and Schwartz (1983), who noted the presence of two individual nebulae, GGD 33a and 33b, and a faint T Tauri star, IRS 1 (now designated as V350 Cep). This T Tauri star was suggested as the parent star of GGD 33a,b because of its proximity and the alignment of the three objects.

Cohen and Fuller (1985) presented spectra of V350 Cep between 3000 and 7500 Å and characterized the star as a strong-lined T Tauri star with an M2 photosphere. Cohen (1985, private communication) reports that the absorption spectrum of V350 Cep is quite variable, with the TiO bands sometimes being invisible, presumably filled in by chromospheric emission. Figure 2(a) presents the spectrum of V350 Cep taken on 14/15 July 1985 at two different vertical scales. The observed fluxes of some of the emission lines in the spectrum of V350 Cep are given in Table II for possible comparison with other data sets and for comparison with the simultaneous spectra of GGD 33a,b discussed below.

Harrington and Lada (1985) and Strom *et al.* (1986) have compared Hα, *V*, *I*, and *R* images of the GGD 33a,b region and concluded that both of these nebulae are purely reflection nebulae. The dichotomy between reflection and emission nebulae is often not clearly resolved by comparing continuum and Hα images because many young stars show strong Hα in emission, making the interpretation of the Hα/continuum ratio ambiguous. Young stars do not generally have [O I] or [S II] lines of large equivalent widths, and thus it may be more appropriate to compare, say, [S II] and continuum images to determine the nature of nebulous objects. Figures 2(b) and 2(c) present the spectra of GGD 33a and 33b, respectively. The observed fluxes of several emission lines are given in Table II. From Fig. 2(b) it is clear that GGD 33a (the nebulosity closest to V350 Cep) has a substantial emission component (note the strong [O I] $\lambda\lambda$ 6300,6363 and [S II] $\lambda\lambda$ 6717,6731 lines). There is also a substantial reflected continuum as evidenced by the red continuum. This continuum shows structure very similar to the continuum of V350 Cep displayed in Fig. 2(a), including a broad maximum near λ 7400 followed by a dropoff to the red near λ 7600, and slight discontinuities near 5100 and 6100 Å. From this it appears safe to conclude that GGD 33a is reflecting the light of V350 Cep and is hence probably associated with that star. The Hα line in GGD 33a must contain a contribution from the reflected V350 Cep Hα line. The equivalent width W_λ of Hα in V350 Cep is 71 Å; the Hα line in GGD 33a has $W_\lambda = 243$ Å. Hence the Hα line in GGD 33a is $\sim$30% reflected and 70% intrinsic. Note that because of the large variability of V350 Cep this comparison is not completely fair—due to the finite speed of light, the reflection we see from GGD 33a is actually a *delayed* version of the spectrum of V350 Cep.

Cohen and Fuller (1985) have used 3 m ITS spectra of GGD 33a,b to place 3σ upper limits on the intensity of Hα in these two objects. Their limit on GGD 33b of 4.5×10^{-15} erg cm^{-2} s^{-1} is consistent with my spectra, but their limit of 6×10^{-16} erg cm^{-2} s^{-1} on GGD 33a is contrary to my observation of $F(\text{H}\alpha) = 3.0\times10^{-15}$ erg cm^{-2}s^{-1}. The reason for this discrepancy is not clear—since most of the Hα flux in GGD 33a is intrinsic to the HH object it is not likely that the Hα line strength has changed significantly in the $2\frac{3}{4}$ yr between the last Cohen and Fuller observation and mine. (The recombination time scales of HH objects are typically between 30 and 200 yr—see Dopita 1978.)

Table III presents limits on the shock parameters of GGD 33a. In particular the upper limit on the reddening is not very interesting. However, the continuum fluxes given in Table IV may be used to estimate an approximate reddening. (Although clearly there are other effects involved, such as the wavelength dependence of the dust albedo in the reflection nebulae, and even the phase delay between the variable spectrum of V350 Cep and the reflected continuum from

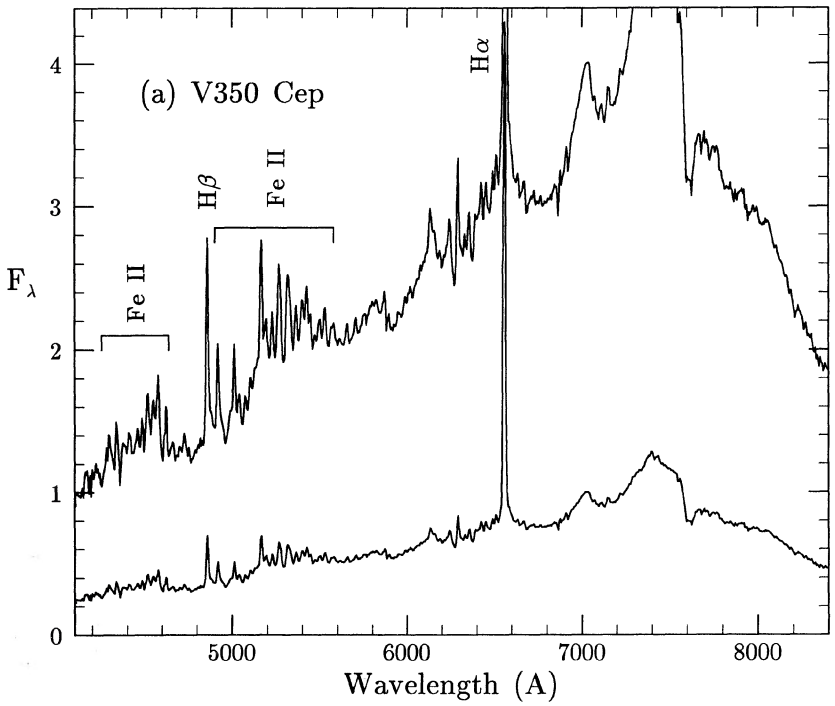

FIG. 2. (a) Spectrum of V350 Cep, the parent star of GGD 33a,b, shown at two scales. The F_λ scale is in units of 10^{-15} erg cm^{-2} s^{-1} Å^{-1} and corresponds to the lower spectrum—the upper spectrum has been multiplied by a factor of 4 to better show the photospheric features and the rich emission spectrum.

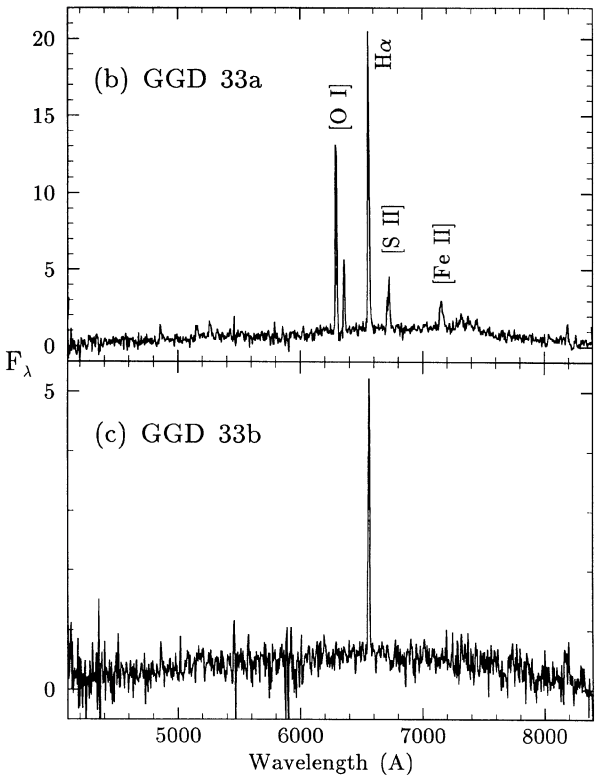

FIG. 2. (b and c) Optical spectra of GGD 33a and 33b. Note the reflected continuum in both objects and the strong Hα lines. The strong forbidden lines of [O I] and [S II] in GGD 33a indicate that this object also has some intrinsic emission. The units of F_λ are 10^{-17} erg cm^{-2} s^{-1} Å^{-1}.

GGD 33a!) The data are somewhat ambiguous, but there is no evidence for a large reddening ($E_{B-V} < 0.25$), indicating that the star and the HH objects are subjected to more or less the same amount of reddening.

The spectrum of GGD 33b presented in Fig. 2(c) shows only Hα in emission along with a red continuum. The equivalent width of Hα in this spectrum is 100 Å, indicating that it is probably ~70% reflected and 30% intrinsic.

As noted by several authors (e.g., Harrington and Lada 1985), the NGC 7129 region is very complex, with two or more overlapping CO outflows, three H_2O masers, and several HH objects. Recognizing GGD 33a as an HH object associated with V350 Cep adds another aspect to the picture, as there is no bipolar CO outflow known to be associated with this star.

c) GGD 34 and 35

Cohen and Schwartz (1983) pointed out that GGD 33a,b, V350 Cep, and GGD 35 all lie on a single line. Cohen and Fuller (1985) note that this alignment may be coincidental in the case of GGD 35, due to its large projected distance of 1.3 pc from V350 Cep. These latter authors also present a spectrum of GGD 35 confirming the HH nature of this object as first reported by Magakyan (1983). Cohen and Fuller also mention that they could not locate an emission-line object at the position of GGD 34 reported by GGD78.

Figure 3(a) [Plate 46] presents a montage of deep, red CCD images of the GGD 34/35 area showing both the GGD 34 and 35 nebulae as well as a curved nebula with a faint detached nebulosity just to the west of GGD 34. This curved nebula was also seen by Harrington and Lada (1985). Figures 3(b) and 3(c) present the CCD spectra of GGD 34 and GGD 35, respectively. The spectra are characterized by low-ionization or neutral species such as [N I], [O I], and [S II], although there is slight evidence for the [O III] λ 5007 line in the spectrum of GGD 34. There also appears to be a faint continuum rising toward the blue in GGD 35, probably due to two-photon emission of hydrogen. Table II contains the emission-line flux measurements from these two spectra.

The curved nebula seen to the west and slightly south of GGD 34 was reported as a reflection nebula by Harrington and Lada (1985).

d) Haro 6-10

Both Elias (1978) and Cohen and Fuller (1985) discuss the nebulous object Haro 6-10, and both papers contain spectra of the object. The object contains a strong red continuum as well as Hα emission and strong forbidden lines of [O I] and [S II]. The ratio of [O III] λ 5007/Hβ is 0.13, indicating a shock temperature of 4×10^4 K according to Dopita's (1977) models, and assuming that the [O III] and Balmer lines are formed in the same region of the nebula. Cohen and Fuller derive a reddening to Haro 6-10 of $E_{B-V} \sim 0.8$ by fitting a shock model to the observed [O III]/Hβ line ratio and comparing the observed Balmer decrement with that predicted by the model. The weak silicate absorption seen in infrared spectra of Haro 6-10 by Elias (1978) indicates an optical depth $\tau_{Si} \sim 0.12$. Using the cali-

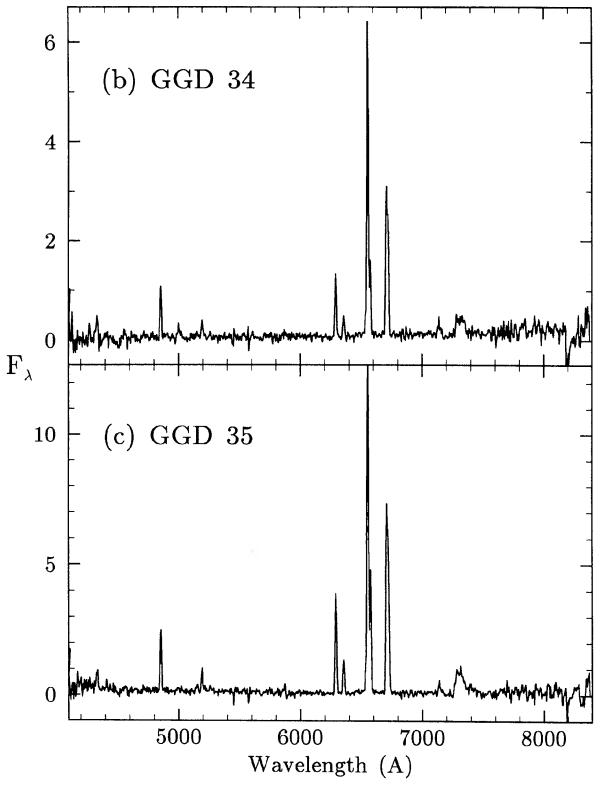

FIG. 3. (b and c) Spectra of GGD 34 and GGD 35. Both have spectra typical of HH objects. The F_λ scale is in units of 10^{-16} erg cm^{-2} s^{-1} Å^{-1}.

bration of Rieke and Lebofsky (1985) for A_V/τ_{Si} and assuming that $A_V = 3.1$, E_{B-V} yields a value of $E_{B-V} = 0.6 \pm 0.1$, consistent with the determination from the Balmer lines. Cohen and Fuller (1985) note that the lack of a strong TiO feature near 6160 Å implies that Haro 6-10 is an early K star. The spectrum presented in Fig. 4 shows a weak TiO feature at this wavelength as well as a well-defined break at the MgH feature near 5175 Å. The bolometric luminosity of Haro 6-10 estimated by Cohen *et al.* (1984) is 6.5 $L_\odot$. Using these three clues it appears that the spectral type of Haro 6-10 lies between K3 III and K5 V. Monochromatic magnitudes determined from Fig. 4 are $B = 19.2$, $V = 17.2$, giving $(B-V)_{obs} = 2.0$. Assuming an intrinsic $(B-V)_0 = 1.22$ (obtained from the tables in Fitzgerald 1970), this implies a reddening of $E_{B-V} = 0.78$. This is quite consistent with the determination by Cohen and Fuller (1985) and the value derived above from the silicate feature.

Spectropolarimetry of this object indicates a polarization of $3.49 \pm 0.07\%$ at p.a. $66 \pm 1°$. The data show that Hα is polarized the same as the continuum; the results for [S II] and [O I] are the same, but with less confidence. This indicates that as we see this object the continuum from the star and the emission lines from the nebula are subject to the same polarization mechanisms. Because of the faintness of Haro 6-10 in the blue it is difficult to characterize the wavelength dependence of the polarization, and hence it is hard to say whether the polarization looks more like transmission polarization through aligned dust grains or reflection by dust. However, both possibilities merit attention. Generally, reflection nebulae are characterized by much larger polarizations, often approaching or exceeding 50% (e.g., Schmidt and Miller 1979; Schmidt, Angel, and Beaver 1978). For a finite slit size the measured polarization will be the average across the nebulosity observed; for a face-on, circularly symmetric nebula the resulting polarization from a centered slit will be zero. In fact the nebulosity associated with Haro 6-10 is rather small and is almost circularly symmetric. For a circularly symmetric (i.e., disk-shaped) reflection nebula seen at a tilt, the resulting polarization position angle will be perpendicular to the projected axis of the disk. The position angle of 67° would then indicate that the axis of the disk would lie along p.a. − 23°, which is close to the p.a. which Cohen and Schwartz find for the infrared source. On the other hand, the position which Elias (1978) finds for the infrared source is consistent with there being no displacement between the optical nebulosity and the infrared source. Under this latter assumption it becomes easy to explain the polarization of Haro 6-10 as transmission polarization by aligned dust grains. Serkowski, Mathewson, and Ford (1975) present a plot of E_{B-V} vs p (polarization) for a large number of stars which have significant interstellar polarization (and reddening). The ratio of E_{B-V}/p for Haro 6-10 in this diagram is found to be typical of interstellar reddening and polarization. Evidently the optical object Haro 6-10 is a star surrounded by nebulosity, both of which are subjected to interstellar reddening and polarization. In this context it is noteworthy that Bieging, Cohen, and Schwartz (1984) determined that the radio source they observed at 4885 MHz is coincident with the optical object. Hence it is not clear that Haro 6-10 is really an HH object in the usual sense of the term (indicating a relatively isolated shock-excited emission nebula). There is no evidence for a preferred outflow direction and the nebulosity appears to surround the star more or less symmetrically. Cohen and Fuller (1985) also reported a very small radial velocity, and a density (from the [S II] lines) which is higher than most (but not all) HH objects. Also, Edwards and Snell (1983) found no evidence for high-velocity molecular outflow around Haro 6-10.

Elias (1978) and Strom *et al.* (1986) note the existence of two small nebulosities to the southwest of Haro 6-10, defining a position angle of ~65%. The coincidence of this direction with the position angle of the optical polarization is very

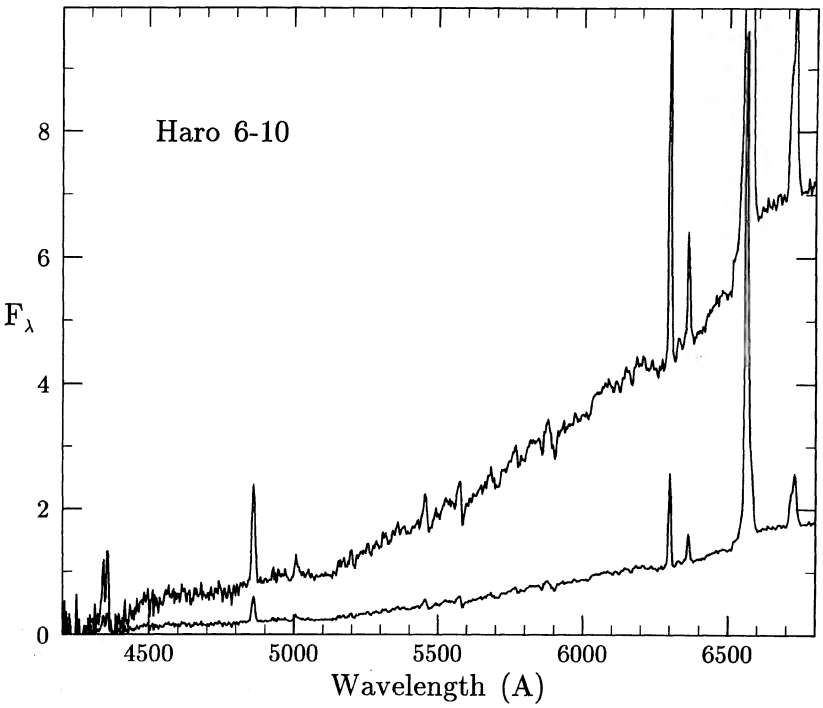

FIG. 4. Spectrum of Haro 6-10, plotted at two scales. The F_λ scale is in units of 10^{-15} erg cm^{-2} s^{-1} Å^{-1} and corresponds to the lower plot—the upper plot is magnified by a factor of 4. The continuum of this object is intermediate in spectral type between K3 III and K5 V and is reddened by $E_{B-V} = 0.78$. There is a spurious emission feature in this spectrum and in the spectrum of HH 40 (Fig. 5) due to poor subtraction of the mercury night-sky line at 4358 Å—it can be seen blended with H$\gamma\lambda$ 4301.

suggestive. If the two nebulosities represent one side of a bipolar outflow associated with Haro 6-10, then the polarization indicates that the polarizing grains may be aligned with that axis. It is quite possible that this position angle defines the direction of the local magnetic field in the cloud near Haro 6-10, which may also affect the outflow direction.

In comparing the numbers in Table II with previously published data by Cohen and Fuller (1985) and Elias (1978) it was found that the Hα/Hβ ratio and other line ratios were significantly different between the sets of data. In particular, while the ratio of Hα/Hβ is 8.4 in Elias's 1978 spectrum, Table II gives Hα/Hβ = 21. Cohen and Fuller (1985) do not cover the Hβ region, but for the Elias data, the Cohen-Fuller data, and Table II the Hα/[O I] ratios are 1.9, 2.4, and 5.6, respectively. Of course it is possible that the forbidden lines and the Balmer lines arise in spatially distinct regions, so that data sets obtained with different apertures or different seeing conditions will have different Balmer-to-forbidden line ratios. But even the [S II]/[O I] line ratios are different: 0.49, 0.84, and 0.89 for the Elias, Cohen-Fuller, and present data sets. Haro 6-10 is known to vary in the infrared (Elias 1978), so that the most likely explanation for these differences is a combination of aperture effects and an intrinsic variation of some emission-line component. If one uses the observed Hα/Hβ ratio from Table II and assumes the intrinsic Hα/Hβ ratio from Table III, one derives a visual extinction of $E_{B-V} = 1.6$ (Table III), substantially higher than the continuum extinction derived above. Presumably, then, there is an Hα emission region which is more highly reddened than the stellar light and which has varied between 1978 and 1985. Further monitoring of Haro 6-10 would certainly be desirable.

e) HH 40

HH 40 is a small, bright nebulosity in Orion. Figure 5 presents the spectrum of HH 40, showing that this object has a relatively high excitation ([O III] λ 5007/Hβ = 0.24, $T = 20\times10^4$ K from Table III). Even so, [N I] λ 5199 is visible, as are several Fe II lines. The continuum is very weak and is blue, indicating two-photon emission. Mundt *et al.* (1984) have demonstrated that HH 40 and HH 33 are connected by a narrow bridge of emission, a feature also visible on the Palomar Sky Survey. These authors speculate that HH 33 and HH 40 represent two ends of a collimated jet which points back to the parent star. Cohen and Schwartz (1983) searched for infrared sources in this region and proposed that one of three stars with infrared excesses (IRS 3, IRS 4, and IRS 7 in their notation) was the parent star. These stars all lie to the southeast of HH 33/40, along the jet axis. However, the high excitation of HH 40 may indicate that it is the jet's "working surface," and not HH 33. In this case HH 40 would be the object furthest from the parent star, which would lie towards the northwest of HH 33/40. A search of the *IRAS* point-source catalog reveals that there is an infrared source, IRAS 05325 − 0616, 6′ to the northwest along the jet axis. Mundt *et al.* found very low radial velocities for HH 33 and HH 40, indicating that their motion may lie mostly in the plane of the sky. In this case it would be interesting to try to determine proper motions for these two HH objects. There is apparently very little (if any) high-velocity molecular gas associated with these objects, as shown by Edwards and Snell (1983).

f) RNO 40

Object 40 in Cohen's (RNO) list lies in a dark obscuration in Orion. Proper-motion studies (Jones *et al.* 1984) indicate that the object is moving towards the west at a velocity of $\sim$90 km s^{-1}, away from an infrared source 2′ to the east. This infrared source is their proposed parent star for RNO 40. The spectrum of RNO 40 (Fig. 6) shows a wealth of emission lines, including the usual HH lines of [O I], [S II], and [N I]. As shown in Table III, the [O III] lines indicate a

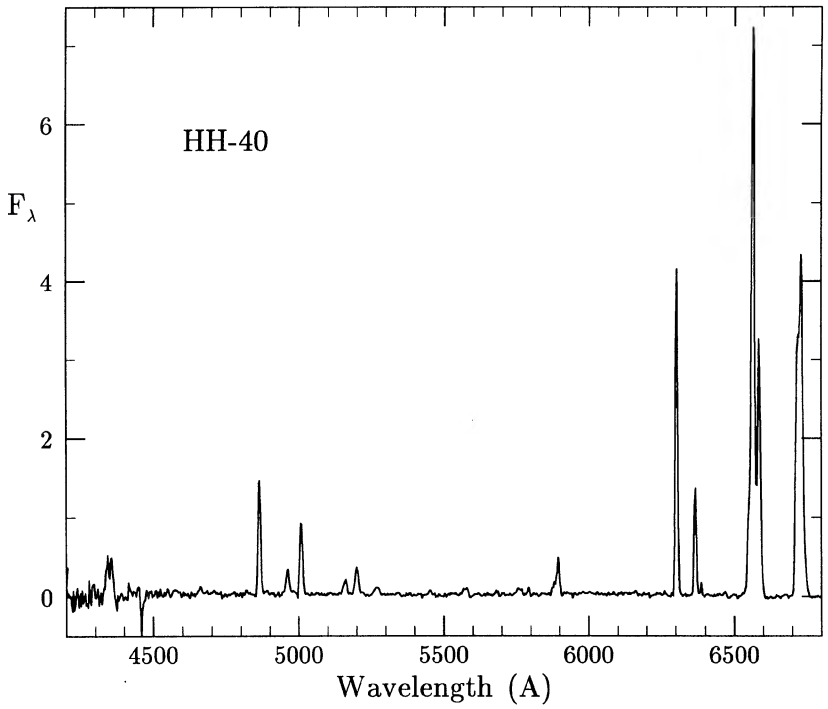

FIG. 5. Optical spectrum of the high-excitation object HH 40. Note the relatively strong [O III] lines at $\lambda\lambda$ 4959, 5007. The units of F_λ are 10^{-15} erg cm^{-2} s^{-1} Å^{-1}.

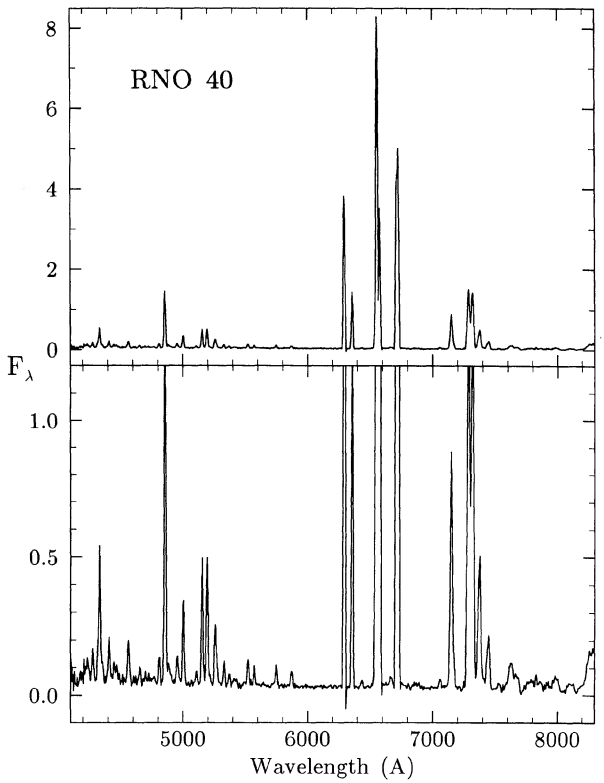

FIG. 6. Spectrum of RNO 40. The lower panel shows on a magnified scale the rich [Fe II] spectrum of this bright HH object. The units of F_λ are 10^{-15} erg cm^{-2} s^{-1} Å^{-1}.

relatively high excitation ($T = 20\times10^4$ K). In Table V, identifications and fluxes for most of the weak lines in RNO 40 are listed. The continuum in RNO 40 is blue, again suggesting two-photon emission.

IV. DISCUSSION

The main objective of this paper is simply to present some optical observations of some known and suspected HH objects and their parent stars. However, there are some data presented here which are rather interesting and warrant further discussion. The spectrum of SSV 13 presented in Fig. 1 is quite unusual for an HH object. Unfortunately, due to the large amount of extinction towards this object the accessible wavelength region is severely restricted and includes only four emission lines of interest—the [O I], Hα, [S II], and [Fe II] lines. However, the relative strengths of these lines are very peculiar. The relative strengths of emission lines in HH-type shocks may be affected by four principle factors which I will discuss. These are the excitation (or shock temperature), the density, the fraction of hydrogen that is in atomic form, and the filling factor of the high-density material. The latter is included in the discussion because, as Brugel, Böhm, and Mannery (1981) have shown, there are apparently two different density regimes in many HH objects.

Of course, with four line strengths and four "free parameters" it is usually possible to create a perfect fit. However, I shall not attempt such a fit but will instead discuss qualitatively the spectrum of SSV 13. One of the peculiarities of the SSV 13 spectrum is the small [S II] flux. In the context of the four factors discussed above this might imply that the shock is a high-excitation shock, that the density is high, or that the filling factor of the high-density gas is large. One effect of a high excitation is also a small ratio of [O I]/Hα, which is *opposite* to that seen in SSV 13. A high density might explain the small flux in the [S II] lines while still maintaining a substantial [O I] line strength, due to the different critical densities of the lines (the critical densities being defined as the density at which collisional de-excitation becomes comparable to collisional excitation). DeRobertis and Osterbrock (1984) give values for the critical densities of the [S II] λ 6717, λ 6731, and the [O I] λ 6300 lines as 1.5×10^3, 3.9×10^3, and 1.8×10^6 cm^{-3}, respectively. Hence a density intermediate between, say, 10^4 and 10^6 cm^{-3} will destroy the [S II] level populations without also quenching the [O I] lines.

The [O I]/Hα ratio is relatively large, indicating that the shock is low excitation, and that consequently much of the hydrogen is still locked up in molecular hydrogen. For very low-velocity shocks the [S II]/[O I] line ratios do not change very much (Jones and Cohen, unpublished data), so that this ratio might be useful as a density-sensitive diagnostic in cases where the shock velocities are low and the gas has a density between 10^4 and 10^6 cm^{-3}. Another peculiarity in the SSV 13 spectrum is the very strong [Fe II] λ 7155 emission line. At first one might think that this is due to the destruction of dust grains in the shock and the subsequent enhancement of the metal abundances in the SSV 13 region. However, as Brugel *et al.* (1981) and Böhm and Brugel (1979) point out, the [Fe II] and [Fe III] lines in some well-observed HH objects are consistent with a solar Fe/H abundance. This implies that already in normal HH objects the iron has been released from the dust grains, and we cannot invoke a still higher Fe abundance to explain the SSV 13 line. To further study the problem one can construct a plot of [Fe II]/Hα vs [S II]/[O I], as I have done in Fig. 7. This contains data from this paper as well as from several other authors, as noted in the footnotes to Table VI, where the

TABLE V. RNO 40 line fluxes.

Ion	λ(Å)	Mult.[a]	Flux[b]	Ion	λ(Å)	Mult.[a]	Flux[b]
[Fe II]	4276.83	21F	0.45	[Fe II]	5527.34	17F	1.69
[Fe II]	4287.40	7F	1.20	[O I]	5577.31		1.13
[Fe II]	4319.62	21F		[N II]	5754.8		1.37
Hγ	4340.47		8.07	He I	5875.63		1.05
[O III]	4363.21		1.21	[O I]	6300.30		58.5
[Fe II]	4413.78	7F	2.24	[O I]	6363.78		20.1
[Fe II]	4416.27	6F		[Fe II]	6440.40	15F	0.40
[Mg I]	4571.10		2.98	[N II]	6548.05		14.9
[Fe II]	4814.53	20F	1.43	Hα	6562.82		122.3
Hβ	4861.33		21.1	[N II]	6583.45		44.8
[Fe II]	4889.62	4F	1.23	He I	6678.15		0.61
[Fe II]	4905.34	20F	0.48	[S II]	6716.47		58.2
[O III]	4958.91		1.87	[S II]	6730.85		70.8
[O III]	5006.84		5.02	He I	7065.19		0.60
[Fe II]	5107.94	18F	0.84	[Fe II]	7155.16	14F	17.4
[Fe II]	5111.63	19F		[Fe II]	7172.00	14F	1.41
[Fe II]	5158.78	19F	7.20	[Ca II]	7291.46		35.3
[N I]	5199.6		8.15	[Ca II]	7323.88		30.7
[Fe II]	5261.62	19F	4.84	[Fe II]	7388.18	14F	14.3
[Fe II]	5333.65	19F	1.38	[Fe II]	7452.54	14F	5.27
[Fe II]	5376.45	19F	0.69				

[a] Fe II multiplet number.

[b] in units of 10^{-15} erg cm^{-2} s^{-1}.

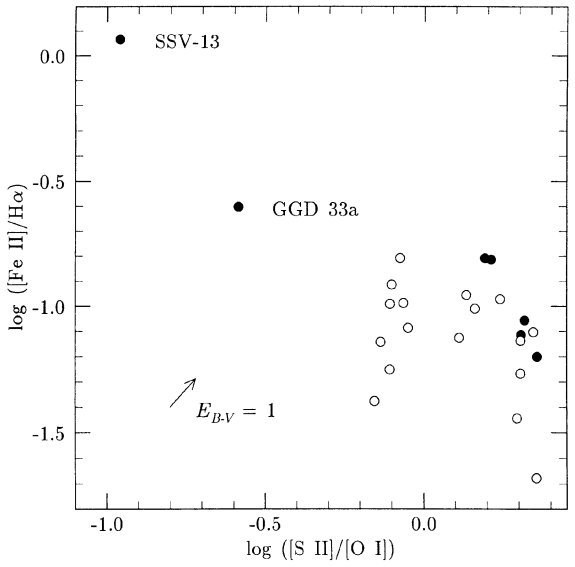

FIG. 7. Plot of [Fe II]/Hα versus [S II]/[O I]. The latter axis may be used as a measure either of density or of the filling factor of a high-density gas in a two-phase model of HH objects. Lower [S II]/[O I] ratios indicate higher density or a larger filling factor of the high-density phase. Dark circles are data points from this paper and light circles are from the literature. All points have been dereddened—the arrow at lower left shows the effects of reddening a point in the diagram by $E_{B-V} = 1$. See the text for a discussion of the significance of this plot.

TABLE VI. Line ratios.

Object	[S II]/[O I]	[Fe II]/Hα
HH-8	1.84	0.067
HH-10	1.88	0.077
HH-11	1.42	0.136
GGD 33a	0.19 – 0.26	0.160 – 0.250
GGD 34	2.49	0.100
GGD 35	2.13 – 2.28	0.057 – 0.063
RNO 40	1.50	0.137
SSV-13	0.071 – 0.083	0.662 – 0.813
HH-1 NW[b]	0.78	0.056
HH-1 NW[c]	0.78	0.102
HH-1 (1)[a]	0.89	0.082
HH-1 (2)[a]	1.36	0.111
HH-2C[a]	0.79	0.122
HH-2G[a]	1.97	0.036
HH-2H[a]	0.73	0.072
HH-2H[b]	0.70	0.042
HH-3[a]	2.27	0.021
HH-24A[a]	2.22	0.079
HH-24A[b]	1.29	0.075
HH-32[b]	1.74	0.107
HH-32A[a]	0.84	0.156
HH-32B[a]	1.45	0.098
HH-40[a]	2.02	0.073
HH-46S[a]	0.86	0.103
HH-47[a]	2.02	0.054

[a] Dopita (1978).
[b] Brugel, Böhm, and Mannery (1981).
[c] Schwartz (1976).

values of the ratios are collected. The flux ratios obtained from Table II were dereddened by the values of E_{B-V} given in Table III; for HH 8 and HH 10 the value of E_{B-V} appropriate to HH 11 ($E_{B-V} = 0.54$). For objects in which only an upper limit to E_{B-V} is available, a range of ratios is given in Table VI, corresponding to the maximum allowable reddening and no reddening. The ratios taken from the literature were already dereddened by the authors. Figure 7 also shows the trajectory along which a point would move in the diagram if the reddening were wrong. The effect is rather small for any reasonable reddening values.

The [S II]/[O I] ratio used in Fig. 7 may be regarded as an indicator of either density or filling factor. The implications of the other axis are less clear, because the Hα strength is affected by the excitation and the [Fe II] strength is affected by the density at some point. The point at which the [Fe II] line is collisionally de-excited is not known because the atomic parameters for the Fe^+ ion are not at all well determined. In any case the presence of Hα in the denominator of the ratio does not qualitatively change the plot—plotting [Fe II]/[O I] vs [S II]/[O I] yields a similar plot. We can still make some observations about the data points in this plot. First of all, the majority of the points lie in a cluster in the lower right-hand side of the diagram, while two data points lie to the left. These two points also seem to show larger [Fe II]/Hα ratios but, as discussed above, it is not clear what this is implying. There appears to be a trend in which a higher density (smaller x value) correlates with a higher [Fe II]/Hα ratio.

The other data point which displays an anomalous [S II]/[O I] ratio, as well as an anomalous [Fe II]/Hα ratio, is GGD 33a. Now there is one thing which both the SSV 13 and GGD 33a spectra have in common, and that is a strong red continuum. In the case of GGD 33a the continuum has been shown (in Sec. III*b*) to be light reflected from V350 Cep. In the case of SSV 13 it is not known whether the continuum is the star itself or a reflection nebula very close to the star. A possible explanation for both the presence of reflection (i.e., the presence of a substantial amount of dust) and the anomalous line ratios in these two HH spectra may now be formulated. Whereas most HH objects represent shocks from material moving through a relatively low-density medium, it might be expected that some HH objects are material running into a very dense ambient medium. This dense medium would not only have a lot of dust in it, but it would also provide a solid "wall" of material. Then the shock would be passing through a high-density region with a filling factor of unity, and the [S II] line strength would decrease. It is possible that in SSV 13 the density of the material is close to the critical density of the [O I] line, 1.8×10^6 cm^{-3}, and the [O I] lines are partially quenched by collisional de-excitation. If the [Fe II] line has a higher critical density, it could then remain unaltered in strength while the [S II] and [O I] lines are decreased in strength and the Hα line is weaker because only a portion of the hydrogen has been converted from molecular hydrogen to atomic hydrogen.

Confirmation of the high density in GGD 33a may be found in Table III, where the shock fits to the observed line ratios indicate $\log N > 3.2$. In fact GGD 33a shows the largest ratio of [S II] λ 6731/λ 6717 in Table III, although Haro 6-10 has a comparable ratio. This already indicates that the [S II] lines are being produced in a region with a density close to the critical densities of the lines, implying a significant degree of collisional de-excitation.

Of course it is dangerous to base too much speculation on a correlation depending mainly on only two data points. What one would like is more objects which show reflected continua to see if they lie in the left-hand part of the diagram. One must be very cautious, however, because some part of the Hα line, for example, might be reflected from the parent star. Then the measured [Fe II]/Hα ratio would be too low. The data point corresponding to GGD 33a in Fig. 7 has been corrected for this reflected component by comparing equivalent widths of Hα in the object and in the parent star (see Sec. III*b*). Spectropolarimetry is another, even more reliable, way to remove the reflected components of the emission lines, as demonstrated by Schmidt and Miller (1979) on HH 24E. Unfortunately, HH 24E is almost pure reflection, so that these latter authors did not detect either the [S II] or the [O I] lines, and their wavelength coverage did not include the [Fe II] line. Haro 6-10 has a large value of log N (from Table III) which is close to the critical density of the [S II] lines. Unfortunately, the disagreement between the Hα line fluxes reported by various observers (see Sec. III*d*) indicates that there is probably a variable and/or a spatially distinct Hα source in Haro 6-10, and it is not clear how meaningful the [Fe II]/Hα ratio is in such a situation. Spectropolarimetry indicates that the Hα line is polarized the same as the continuum of the star, which means that any reflected component to Hα is likely to be small. Perhaps a better procedure would be to obtain a spectrum of the nebulosity surrounding Haro 6-10, and to remove any reflected Hα component of *that* spectrum by either the equivalent-width method or by spectropolarimetry.

It must be pointed out that in the light of the above discussion it may be unfair to include the emission associated with SSV 13 and GGD 33a in any list of "classical" HH objects. However, there is not a good definition of an HH object in the literature, and the character of the emission is certainly similar to emission seen in low-velocity shocks. The high density and the probable presence of significant amounts of dust in SSV 13 and GGD 33a may point to a qualitatively different source of the shock emission, for instance as a stellar wind impinging upon the parent molecular cloud.

The author would like to thank Dr. J. S. Miller for the loan of significant amounts of telescope time for this project, and Drs. B. F. Jones and G. H. Herbig for much help and encouragement. This work was partially supported under NSF grant AST 84-06843 and CAL SPACE grant CS 63-85.

REFERENCES

Bieging, J., Cohen, M., and Schwartz P. R. (1984). Astrophys. J. **282**, 699.
Böhm, K. H., and Brugel, E. W. (1979). Astron. Astrophys. **74**, 297.
Brugel, E. W., Böhm, K. H., and Mannery, E. (1981). Astrophys. J. Suppl. **47**, 117.
Cohen, M. (1980). Astrophys. J. **85**, 29 (RNO).
Cohen, M., and Fuller, G. A. (1985). Astrophys. J. **296**, 620.
Cohen, M., Harvey, P. M., Schwartz, R. D., and Wilking, B. A. (1984). Astrophys. J. **278**, 671.
Cohen, M., and Schwartz, R. D. (1983). Astrophys. J. **265**, 877.
DeRobertis, M. M., and Osterbrock, D. E. (1984). Astrophys. J. **286**, 171.
Djorgovski, S. (1985). Publ. Astron. Soc. Pac. **97**, 1119.
Dopita, M. A. (1977). Astrophys. J. Suppl. **33**, 437.
Dopita, M. A. (1978). Astrophys. J. Suppl. **37**, 117.
Edwards, S., and Snell, R. L. (1983). Astrophys. J. **270**, 605.
Elias, J. H. (1978). Astrophys. J. **224**, 857.
Fitzgerald, M. P. (1970). Astron. Astrophys. **4**, 234.
Gyul'budagyan, A. L., Glushkov, Yu. I., and Denisyuk, E. K. (1978). Astrophys. J. Lett. **224**, L137 (GGD78).
Harrington, P., and Lada, C. J. (1985). Astrophys. J. Suppl. **59**, 383.
Haschick, A. D., Moran, J. M., Rodriguez, L. F., Burke, B. F., Greenfield, O., and Garcia-Barreto, J. A. (1980). Astrophys. J. **237**, 26.
Herbig, G. H. (1974). *Draft Catalog of Herbig-Haro Objects*, Lick Obs. Bull. No. 658 (Lick Observatory, Santa Cruz).
Herbig, G. H., and Jones, B. F. (1983). Astron. J. **88**, 1040.
Johnson, H. L. (1967). Annu. Rev. Astron. Astrophys. **4**, 193.
Jones, B. F., Cohen, M., Sirk, M., and Jarrett, R. (1984). Astron. J. **86**, 1404.
Magakyan, T. Yu. (1983). Sov. Astron. Lett. **9**, 83.
Miller, J. S., Robinson, L. B., and Schmidt, G. D. (1980). Publ. Astron. Soc. Pac. **92**, 702.
Mundt, R., Bührke, T., Fried, J. W., Neckel, T., Sarcander, M., and Stocke, J. (1984). Astron. Astrophys. **140**, 17.
Rieke, G. H., and Lebofsky, M. J. (1985). Astrophys. J. **288**, 618.
Sandell, G., and Olofsson, H. (1981). Astron. Astrophys. **99**, 80.
Schmidt, G. D., Angel, J. R. P., and Beaver, E. A. (1978). Astrophys. J. **219**, 477.
Schmidt, G. D., and Miller, J. S. (1979). Astrophys. J. Lett. **234**, L191.
Serkowski, K., Mathewson, D. S., and Ford, V. L. (1975). Astrophys. J. **196**, 261.
Stone, R. P. S. (1974). Astrophys. J. **193**, 135.
Stone, R. P. S. (1977). Astrophys. J. **218**, 767.
Strom, S. E., Vrba, F. J., and Strom, K. M. (1976). Astron. J. **81**, 314.
Strom, K. M., Strom, S. E., Wolff, S. C., Morgan, J., and Wenz, M. (1986). Astrophys. J. Suppl. (in press).

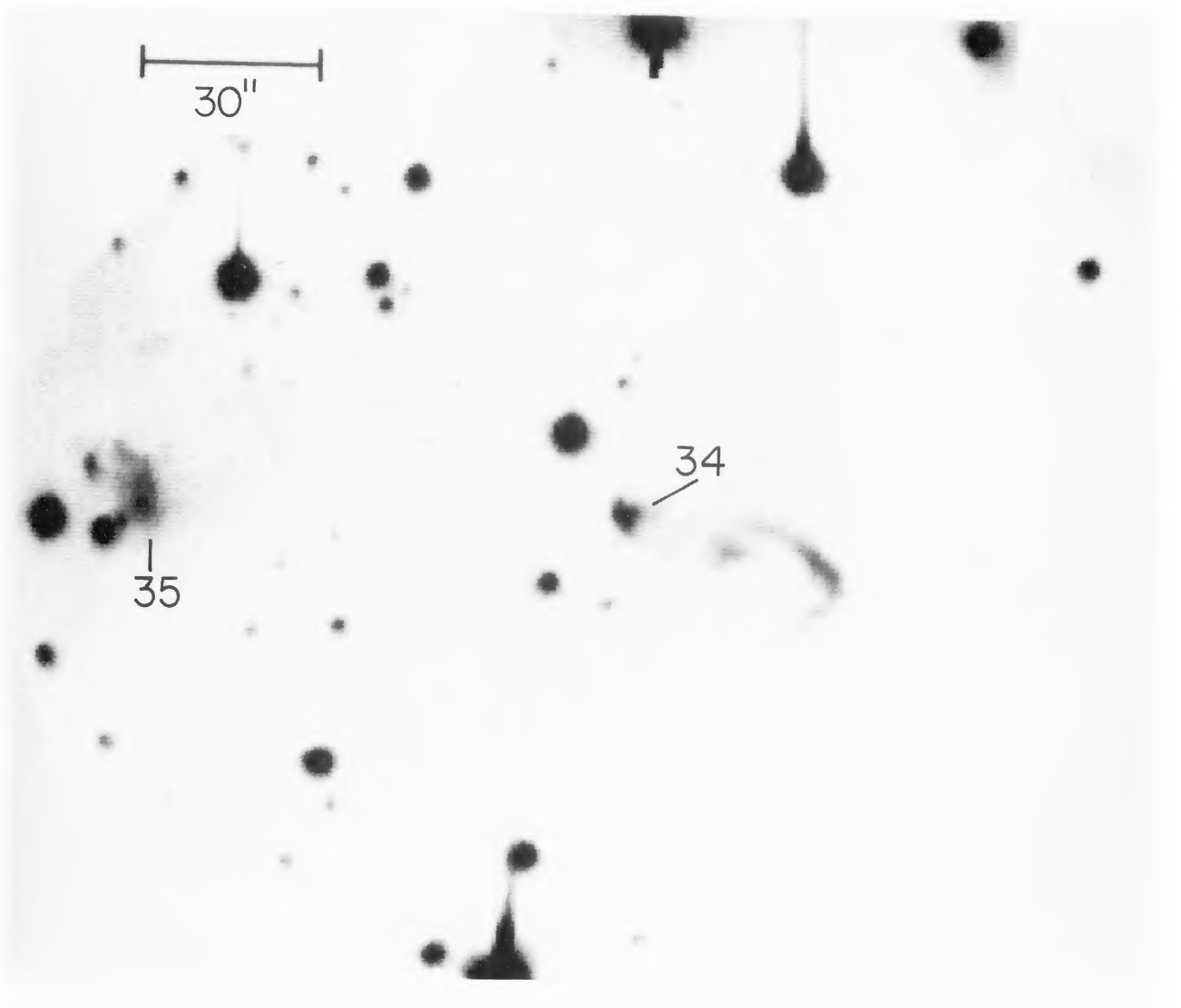

FIG. 3. (a) A montage of CCD images of the GGD 34/35 region. North is up and east to the left—the scale is indicated at upper left. Note the curved nebulosity to the west and slightly south of GGD 34. In the original data this nebulosity appears to be connected to GGD 34 and hence is probably associated with it.

Robert W. Goodrich (see page 889)